

Transactions, SMiRT-25
Charlotte, NC, USA, August 4-9, 2019
Division III

SIMULATING THE THERMOMECHANICAL EVOLUTION OF SFR FUEL SUBASSEMBLIES WITH A COUPLED APPROACH

Acosta Francisco¹, Blanc Victor², Rubiolo Pablo³, Cadiou Thierry⁴

¹ PhD Student, CEA, DEN, DER, SESI, 13108, Saint Paul lez Durance, France. (francisco.acosta@cea.fr)

² Research Engineer, CEA, DEN, DEC, SESC, 13108, Saint Paul lez Durance, France.

³ Professor, University of Grenoble-Alpes, CNRS/IN2P3, 38000, Grenoble, France.

⁴ Research Engineer, CEA, DEN, DER, SESI, 13108, Saint Paul lez Durance, France.

ABSTRACT

We employ a novel methodology to simulate the irradiation of Sodium cooled Fast Reactors (SFR) subassemblies considering the coupling between thermal-hydraulics and thermomechanics, traditionally neglected, to show that this coupling leads to a significant reduction of the stresses and strains of a highly irradiated 7-pin fuel bundle. Additionally, a beam-based finite element model is found to compute swelling and irradiation creep strains – averaged over the fuel cladding's cross section - that agree well with those obtained with a 3D model, but only the latter can resolve the high computed swelling gradients, which are also shown to increase when considering the coupling.

INTRODUCTION

During their irradiation in the core of SFR, the wire-wrapped fuel pin claddings and the hexagonal wrapper tubes that constitute their subassemblies undergo severe geometrical changes under the effects of void swelling and irradiation creep [1], which are temperature dependent phenomena. The resulting fuel bundle deformation induces local temperature perturbations, and it increases its hydraulic resistance, which leads to a reduction of the coolant mass flow rate and a temperature increase. Therefore, since the deformation both depends on and affects the temperature distribution, it results that the thermal-hydraulic and thermomechanical evolution of SFR subassemblies under irradiation are coupled.

Traditionally, this coupling has been neglected since the temperature distribution used as input for the thermomechanical calculations is obtained with thermal-hydraulic simulations using the nominal geometry and low-resolution sub channel codes. In order to improve the accuracy of the subassembly deformation calculations, a new coupled simulation methodology is under development at the CEA [2]. This new methodology uses a Reynolds Averaged Navier Stokes (RANS) model implemented in Star-CCM+ [3] and DOMAJEUR2, an in-house SFR bundle thermomechanical code.

In this work, we show the interest of applying the coupled methodology to study the behaviour of SFR subassemblies under irradiation, from the perspective of the mechanical integrity of the fuel pins during nominal reactor operation. The analysis focuses on the coupling effects on strains and stresses, and on the capability of the RANS model of resolving the high temperature gradients in the fuel pin claddings.

THERMOMECHANICAL EVOLUTION OF SFR SUBASSEMBLIES UNDER IRRADIATION

Phenomena Involved in the Evolution of the SFR Subassemblies

In nominal operation conditions, the main causes of the deformation of SFR subassemblies are void swelling and irradiation induced creep. Void swelling can be defined as the isotropic volume increase

caused by the coalescence and growth of voids within the material, consequence of the irradiation induced mobile defects. It is characterized by having an incubation period during which the volume change remains relatively small, despite the increasing irradiation dose. After a certain incubation dose is reached, the swelling rate grows until attaining a steady state value. The volume swelling rate per dpa (Displacement Per Atom), \dot{g} , can be written as a function of the irradiation dose D in the form given by Equation 1 below:

$$\dot{g} = \frac{\dot{g}_0}{1 + e^{\frac{\Delta g - D}{\delta g}}} \quad (1)$$

Where \dot{g}_0 is the steady state swelling rate per dpa, Δg the incubation dose, and δg the transition dose from incubation to steady state. Due to its isotropy, the swelling strain ϵ_{swe} can be expressed as:

$$\epsilon_{swe} = (1 + g)^{1/3} - 1 \quad (2)$$

Both the incubation dose and the steady state swelling rate depend on the material temperature. Swelling affects mainly the pin claddings and spacer wires, since the martensitic alloys employed for the hexagonal wrapper tube – also called hexcan - show an excellent swelling stability [4].

The irradiation damage greatly enhances the mobility of crystallographic defects such as vacancies, interstitials and dislocations, which gives place to a phenomenon called irradiation creep. It can be defined as the isochoric irreversible strain of a material under the effect of stresses, it can be orders of magnitude higher than thermally induced creep, and it can manifest at temperatures at which the latter is negligible. The irradiation creep equivalent strain rate $\dot{\epsilon}_{eq}^{irr. creep}$ [1/dpa] can be expressed as a function of the equivalent stress σ_{eq} and the volume swelling rate as indicated by Equation 3:

$$\dot{\epsilon}_{eq}^{irr. creep} = (1 + 2\alpha\sigma_{eq})K\sigma_{eq} + \alpha\sigma_{eq}\dot{g} \quad (3)$$

Where K is the temperature dependent creep compliance parameter, and α the creep swelling coupling coefficient that is considered to take a constant positive value.

For the reference cladding austenitic steel of French SFR, the steady state swelling strain rate [1/dpa] and $\dot{\epsilon}_{eq}^{irr. creep}$ are maximal for temperatures in the 485°C-525°C range, as can be seen in Figure 1 a). At higher temperatures, they both have negative partial derivatives with respect to temperature ($\partial\epsilon/\partial T$). The incubation dose increases monotonically with temperature up to about 750°C, which shifts the maximum integrated swelling to slightly lower temperatures (~450°C-490°C), as can be observed in Figure 1 b).

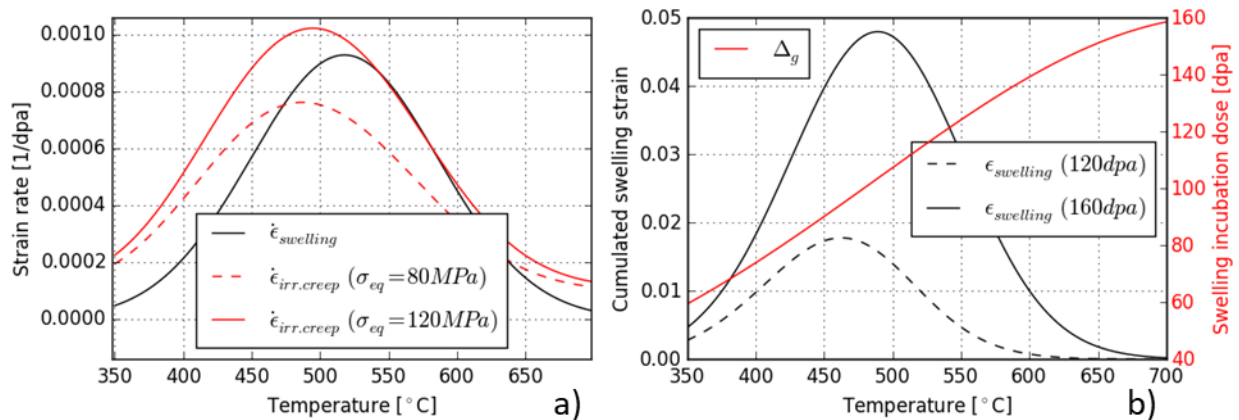


Figure 1: Temperature dependence of swelling steady state strain rate and irradiation creep rate for different σ_{eq} (a), and of the incubation dose and cumulated swelling strain for different irradiation doses (b).

SFR Bundle Deformation Mechanisms and Mechanical Design Criteria

The high fast neutron flux to which the fuel pins are exposed, added to the high temperatures and increasing internal fission gas pressure during their irradiation, activate the aforementioned swelling and irradiation

creep. These phenomena lead to a significant strain of the claddings and their spacer wires, which are also subject to thermal expansion. Macroscopically, these strains lead to the bowing of the fuel pins, their helical flexion, the increase in the diameter of the claddings and the wires, and their ovalisation [1], [5].

The bowing appears from the beginning of the irradiation, and it is caused by the differential thermal expansion of the claddings. The associated stresses are low, since the bowing involves the whole length of the fuel pins. As the irradiation proceeds, the differential deformation of each cladding and the spacer wire around it leads to the helical flexion of the pin under the tension of the wire. The contact between fuel pins through the spacer wires, which occurs during normal operation and marks the start of the 2nd phase of bundle interaction, increases the pin helical flexion that helps to accommodate its diametral strain. If the irradiation continues, a time comes where the pins cannot continue flexing and the ovalisation of the cladding's section is the only mechanism available to mitigate the mechanical interaction between pins. This is called 3rd phase of bundle interaction, and is not allowed in normal operation since, with the typical SFR fuel pin geometry, higher forces are required for the ovalisation of the cladding than for its flexion following the wire step.

Since the cladding of the fuel pins constitutes the first containment barrier for the fuel material, and its failure would release radioactive isotopes into the primary circuit, a set of design criteria have been developed to guarantee their physical integrity [6]. Table 1 summarizes the most relevant mechanical design criteria and the failure mechanism each of them addresses. The limiting values presented on Table 1 are similar between the different SFR development programs around the world.

Table 1: Typical mechanical design criteria of SFR fuel bundles.

Criteria	Limiting value	Associated undesired effect
Maximum equivalent stress	< yield point	Plastic instability
Diametral increase	< 7%	Insufficient cooling + 3 rd phase of bundle mechanical interaction
Volume swelling	< 6%	Embrittlement of austenitic steel
Cumulative creep-rupture damage factor (CDF)	< 0.2-0.3	Creep rupture under the effect of internal pressure
Thermal creep strain	< 0.2%	Creep rupture

Typical Thermomechanical Models Employed to Verify the Design Criteria

A key part of the design process of the SFR fuel subassemblies consists on conducting numerical simulations to verify that the design criteria are respected during nominal operation and in some accidental scenarios. A widely adopted approach consists on the use of finite element methods to model the thermomechanical evolution of one isolated fuel pin, including the cladding and the fuel pellets it contains, as well as the pellet cladding interaction. Such simulations are typically conducted with a 1D1/2 axisymmetric representation of the fuel pin, which is divided into several axial slices which thermal evolutions are coupled by the heat transported by the coolant. This modelling strategy is employed, for example, in the fuel performance code GERMINAL currently under development at the CEA [7].

A different kind of approach exists to model the entire fuel bundle, in order to include the effects of the mechanical interactions between fuel pins, and between pins and the hexcan. In order to avoid an excessively high computational cost, in this approach the mechanical interactions between the fuel pellets and the cladding, usually very limited during normal operation, are not considered. Additionally, the meshing employed is either less refined, or a beam-based representation of the bundle is adopted. Examples of this are the BAMBOO code [8], and the bundle thermomechanical code DOMAJEUR2, developed by the CEA and employed in the present work.

In DOMAJEUR2, which is based on the finite element analysis code CAST3M [9], the quasi-static thermomechanical evolution of the fuel pin claddings, the spacer wires, and the hexcan is modeled by a finite element representation. The effects of void swelling, and irradiation and thermal creep under the

action of the internal fission gas pressure are considered by means of experimentally determined laws. The thermal expansion of the materials and the contacts between fuel pins and between the pins and the hexcan are also considered. Models with different geometrical representations are implemented in DOMAJEUR2 (described in the dedicated section below), ranging from a fully 3D model that employs volumetric finite elements to a beam-based model.

NEW COUPLED METHODOLOGY FOR THE SIMULATION OF SFR SUBASSEMBLIES

Implemented Coupling

Traditionally, the temperature distribution of the fuel pin claddings is computed with low resolution codes (e.g. subchannel codes) in a geometry with as-fabricated dimensions, and it is assumed constant during the irradiation. A previous work exists where a subchannel code was coupled with BAMBOO [10]. The methodology employed in this paper is based on a coupled resolution using a subassembly CFD RANS model implemented in the commercial code STAR-CCM+ and a SFR bundle thermomechanical model using the code DOMAJEUR2 [2]. In this novel approach, the cladding temperature distribution is computed by means of a detailed RANS approach, in which - additionally - the diametral strain of the claddings is explicitly considered in the simulations conducted to compute the temperature field in the deformed geometry. Moreover, the sodium mass flow rate reduction associated with the bundle deformation is also taken into account [2] [11].

For simplicity, in this work we consider a linear time evolution of the cladding temperature between the distribution computed in the non-deformed bundle and the one obtained in the fully deformed bundle at its End Of Life (EOL), and this temperature evolution is used as input for DOMAJEUR2. The coupled calculations are iteratively performed and, in each iteration, the thermomechanical simulation of the bundle irradiation is conducted using the linear cladding temperature evolution determined in the previous iteration. The deformed geometry obtained with DOMAJEUR2 is then used to compute the bundle EOL temperature distribution with the CFD model. This new temperature distribution is used to update the time evolution of the cladding temperature for the next iteration. Convergence is determined when the difference in the EOL strain state of two successive iterations falls below a specified tolerance. Only a few iterations (<5) are typically required.

Thermomechanical Models Employed

Two different models available in DOMAJEUR2 and described in [2] are employed in this work. The first one uses volumetric finite elements to represent the fuel claddings and the hexcan, while the wires are represented by beam elements. The potential contact points between adjacent fuel pin claddings and between claddings and the hexcan, consequence of the bundle deformation, are linked by elastic gap elements. Before contact occurs, they have almost null stiffness, which takes an extremely high value when these elements are activated by the contact. The nonlinear viscoplastic nature of the crushing of the claddings is thus represented by the models of the volumetric finite elements that constitute them.

The second model here employed relies on special 1D hollow beam finite elements, which allow considering the effects of an internal pressurization, to represent the fuel claddings, while shell elements are used for the hexcan. The potential contact points mentioned above are linked by beam finite elements that include an *ad hoc* model to estimate the stress and strain state of the cladding at its internal radius in the positions where contact occurs [9]. This is the point more susceptible to being damaged by thermal creep and, since it has a high order dependence on the stress, a very high accuracy is required to properly compute it. The 3D model evoked above could be employed to this end, but the finesse of the meshing required for the simulation of entire SFR fuel bundles is currently extremely costly in terms of computational power. It is precisely to overcome this limitation that the special beam element has been developed.

The 1D model of the contact elements describes the elasto-viscoplastic crushing of the cladding under the contact between fuel pins, and between the pins and the hexcan. It considers the effects of thermal expansion, swelling, creep, and the modification of the structural rigidity of the cladding's section due to its ovalisation. Under these conditions, the model computes the strain and stress tensor in the inner radius on the cladding by means of stress and strain concentration factors, which depend on the ovalisation and are determined with very detailed elastic finite element simulations of the crushing of a fuel cladding [9].

As it will become apparent later, it is important to highlight that only the 3D model is currently capable of considering the high temperature gradients that the claddings are subject to.

APPLICATION CASE

Irradiation of a 7-Pin SFR Fuel Bundle. Case Description

In this work, we analyse the evolution of a 7-pin fuel bundle irradiated to up to a maximal dose of 165 dpa (close to the maximum dose reached in PHENIX subassemblies) with characteristic dimensions and boundary conditions, presented in Table 2, representative of a 4th generation SFR design [4]. One of these characteristics is the fertile blanket in the central region of the heated column, the effect of which can be observed in the irradiation dose and linear power profiles employed for the simulations conducted here, presented in Figure 2 along with the cross section of the bundle and the pin naming system.

The 3D and the beam-based thermomechanical models were employed to conduct coupled simulations of the subassembly. In the 3D model, every cladding is subdivided in 144 axial slices, each of which is represented with a combination of 13 cubic and prismatic elements (1 element in the cladding thickness) with quadratic basis functions. In the 1D model, each cladding is represented by 144 beam elements. The total number of elements used for the fuel pins and the hexcan with the 3D and 1D models are 18447 and 4433, respectively, and 860 contact elements are used in both cases. The whole length of the fuel bundle is simulated with DOMAJEUR2, while only the heated column, where the irradiation dose is high enough to induce significant deformation, is represented in the CFD model using over 2 million cells.

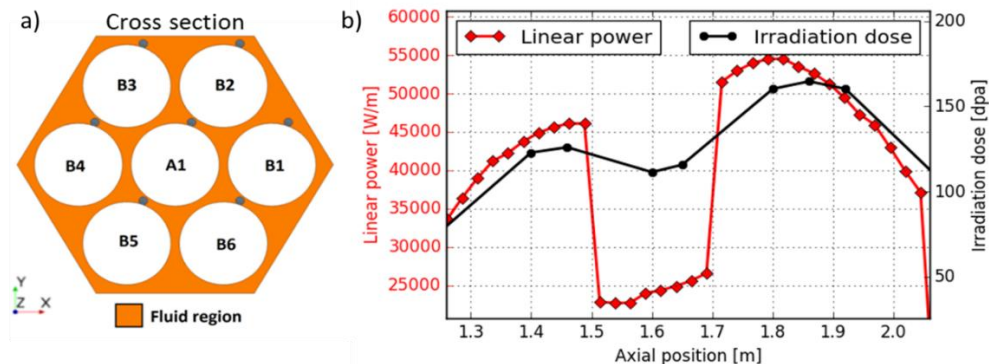


Figure 2: Cross section of the 7-pin bundle (a), and dose and linear power profiles employed (b).

Table 2: Key geometrical and thermal-hydraulic parameters of the simulated 7-pin bundle.

Parameter	Value
Fuel pin length	2.136 m
Heated column length	0.8 m (z = 1.261 m to z = 2.061 m)
Fuel pin pitch	10.8 mm
Fuel pin external diameter	9.7 mm
Spacer wire diameter	1.0 mm
Spacer wire helix step	180 mm

Maximum linear power	550 W/cm
Mass flow rate in nominal conditions	1.2 kg/s
Inlet sodium temperature	400 °C
Hexcan plate to plate distance	30.6 mm

Coupling Effects on Swelling and Creep Strains: Full 3D vs Beam-based Finite Elements

The use of a CFD RANS approach allows capturing the complex sodium flow patterns produced by the SFR bundle geometry, including the local effects caused by the spacer wires. This is illustrated in Figure 3, where the computed cladding temperatures for six different azimuthal angles are presented for the central pin A1 (a) and a peripheral pin, B2 (b), in the non-deformed geometry, along the length of their heated columns. Each profile results from averaging, at each axial position, the computed temperatures over one sixth of the circumference of the cladding. This practice constitutes the systematic post-processing done to each CFD simulation needed to then generate the temperature evolution used as input for DOMAJEUR2.

In the deformed bundle, the increased hydraulic resistance reduces the coolant mass flow rate, leading to an overall temperature increase. In addition, the local hydraulic diameter reduction caused by the cladding diametral strain is more penalizing for the central than for the peripheral subchannels, which are larger. A previous work shows that, when these factors are taken into account in the coupled simulations, the sodium outlet temperature of the 7-pin bundle increases by 30°C, and the temperature gradients of the peripheral pins by about 50% [2]. As can be seen in Figure 3 for the nominal geometry, these gradients are more significant for the peripheral pin since, contrary to the central pin, it is facing the colder hexcan, on one side, and the hotter central subchannels, on the other.

In the cladding temperature range of the upper part of the heated column ($T > 490^\circ\text{C}$), we have $\partial\varepsilon/\partial T < 0$ for both $\varepsilon_{swelling}$ and $\varepsilon_{irr\ creep}$. Therefore, the temperature increase induced by the bundle deformation acts as a negative feedback on swelling and creep strains. This can be seen in Figure 4, where the EOL swelling strain and the creep hoop strain, averaged over the cladding's cross section, are presented for the central pin A1 (a and c respectively) and for the peripheral pin B2 (b and d), as computed by a non-coupled and a coupled simulation. The results obtained with the DOMAJEUR2 model that employs volume finite elements (3D) as well as with the beam-based model (1D) are presented. In the 3D model, the six temperature profiles obtained for each fuel pin with the CFD simulations are employed to interpolate the temperature, at each axial position, over the 13 elements within the cladding's cross section. On the beam-based model, however, only one average temperature per axial position can be considered.

As can be observed in Figure 4, the axially heterogeneous fuel pin concept, that includes a central fertile blanket, leads to swelling and irradiation creep profiles with two distinct maxima each. In the lower part of the heated column, the irradiation creep strain is dominant, while the contrary is true for the upper part. Additionally, the deformation of the peripheral fuel pin is superior to that of the central pin due to its lower temperature that, in the upper half of the heated column, favours both swelling and irradiation creep.

Concerning the effects of the coupling, it can be noted that they affect the swelling more than the creep strain, and that their impact is maximal for the central pin (Figure 4 a), where the swelling strain reduction reaches 30%. The strain reduction due to the coupling is higher in the upper part of the heated column, where the temperature increase induced by the deformation and $\|\partial\varepsilon/\partial T\|$ are both higher.

Additionally, the swelling and creep strains obtained with the beam-based model are in very good agreement with the strains computed by the 3D model (averaged over the cross section of the cladding), despite the fact that only the 3D model considers the azimuthal temperature gradients. In particular, the beam model predicts very well the maximal swelling and creep strains averaged over the claddings circumference, which are the main contributors to its diametral strain. This is particularly important since the diametral strain of the cladding induces the other bundle deformation mechanisms described before, leading to the mechanical contact between the fuel pins. The stresses associated to the mechanical contacts might compromise the integrity of the claddings and are thus evaluated next.

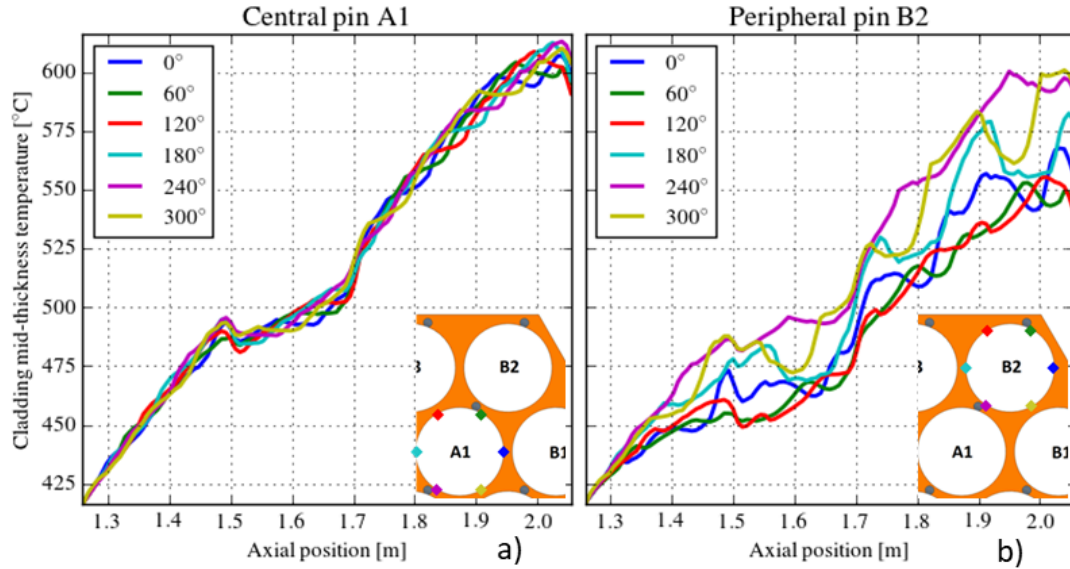


Figure 3: Cladding mid-thickness temperature distribution of the central (a) and a peripheral (b) pin in the non-deformed geometry. Each profile corresponds to a different azimuthal angle.

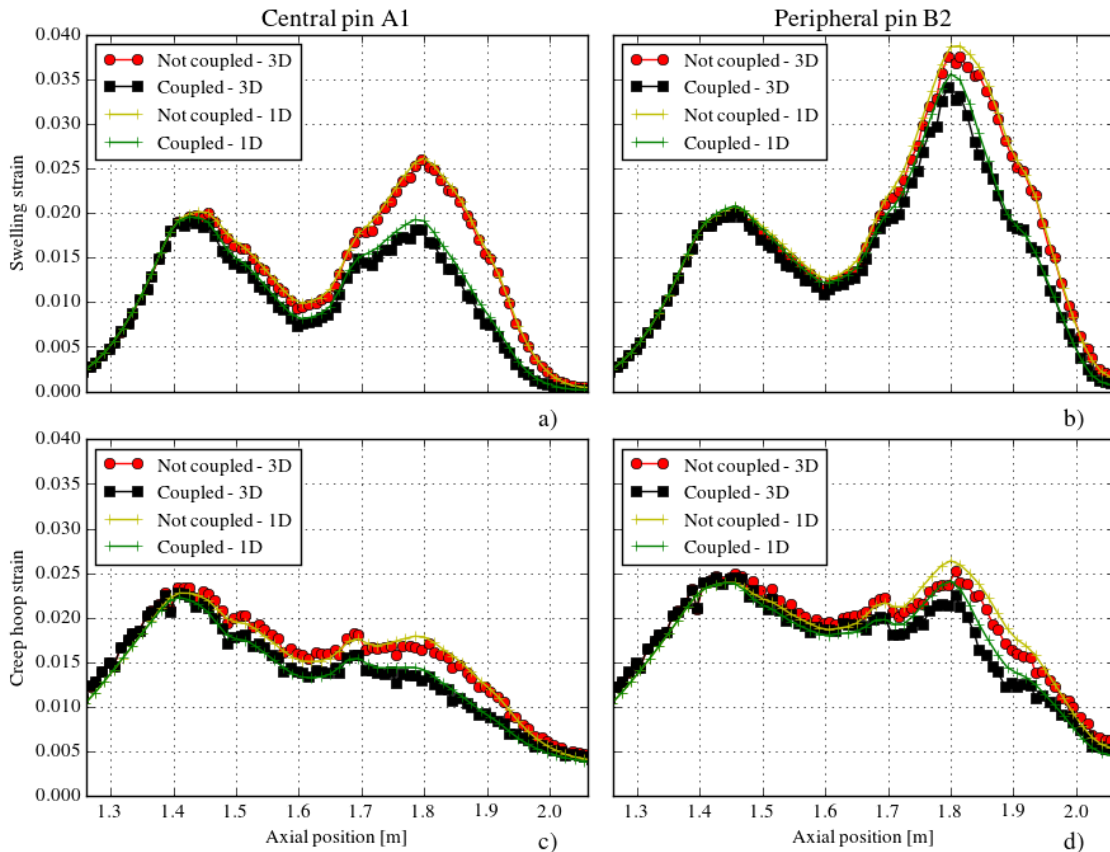


Figure 4: EOL axial average swelling and creep strain profiles of the central (a and c) and a peripheral pin (b and d), computed with the 1D and the 3D finite elements models with and without coupling.

Coupling Effects on the Stress State of the Claddings

We showed how considering the temperature perturbations induced by the deformation leads to a reduction of the swelling and the irradiation creep of the claddings, thus to a reduction of their diametral strain. Since the latter is the driving force for the mechanical interactions between fuel pins and between pins and the hexcan, the predicted mechanical loads of these contacts are also reduced in the coupled simulations with respect to the simulations using the non-coupled approach.

To illustrate this, the equivalent von Mises stress calculated by the contact elements, with and without coupling, are presented in Figure 5 a) for the central pin. The coupling leads to a substantial (~35%) reduction of the maximal equivalent stress, located at the axial position of highest diametral strain; a similar result was obtained for the peripheral pins. At this axial position, the computed time evolution of the equivalent stress and of the pin *gap*, which is a measure – following one of the hexcan diagonals- of the available space to accommodate the diametral strain of the pins, are presented in Figure 5 b). By definition, the pin *gap* becomes null when contact through the spacer wires starts, which marks the beginning of the 2nd phase of bundle interaction, and $gap \approx -D_w$ - where D_w is the diameter of the spacer wires - indicates the start of the 3rd phase. The second limit depends on the strain of the hexcan and of the spacer wires, and thus varies slightly during the irradiation as can be observed in that figure.

By analysing Figure 5 b), the EOL stress reduction computed with the coupled calculations can be explained by a delay of the 3rd phase of bundle interaction, in which only the cladding's ovalisation can accommodate its increasing diametral strain. The start of this phase is characterized by a rapid increase in the equivalent stress, observed at approximately 1540 days in the non-coupled simulation. In the coupled simulation, this phase - which is not allowed in nominal operation- is not yet reached within the irradiation period considered. Additionally, the first contact-induced stress increase, observed between 1200 and 1300 days, is also retarded by the coupling. It should be noted that this stress increase appears later than the start of the 2nd phase ($gap = 0$). This is because, in this case, the 2nd phase starts with the contact between the hexcan and a peripheral pin, which interacts with the central pin later on.

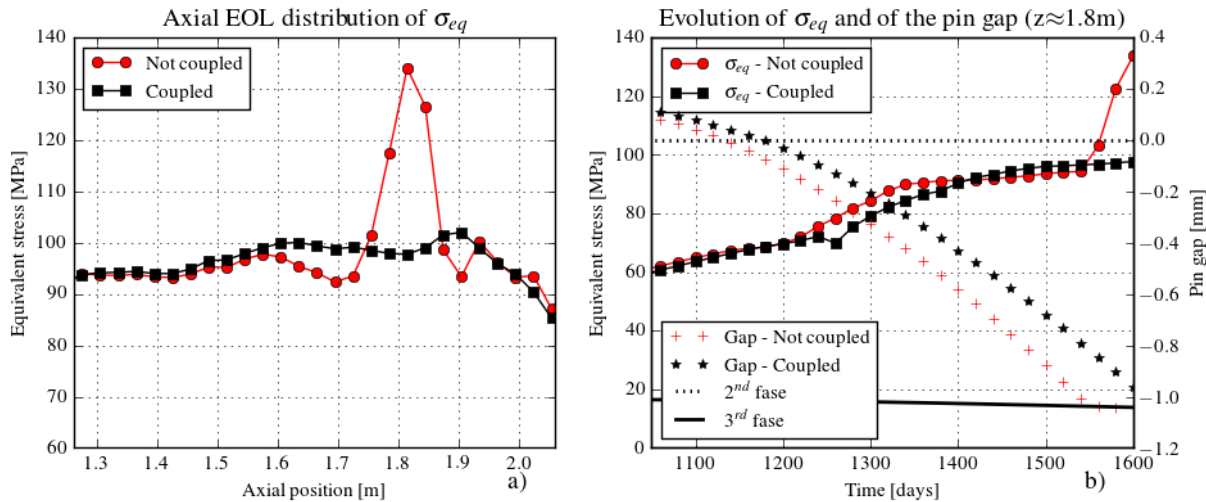


Figure 5: Axial distribution of the equivalent stress (a) and time evolution of the equivalent stress and the pin gap at $z \approx 1.8$ m (b), for the central pin A1.

Cladding Temperature and Swelling Gradients

As described above, void swelling is strongly temperature dependent, thus, under the temperature gradients evidenced by Figure 2, high swelling gradients are established within the fuel claddings, and only the 3D model is able to represent them. To illustrate this, the swelling strain profile along the circumference of pin B2 is presented in Figure 6 a) for an axial position of 1.8 m, where both the swelling strain and its

circumferential gradient are maximal. Both the results obtained with the non-coupled and the coupled simulations conducted with the 3D model are presented. Additionally, in Figure 6 b) and c), the swelling strain distribution within a 1.5 cm axial section of the cladding, at the same axial position, is presented for the non-coupled and coupled simulations, respectively.

As can be observed in Figure 6 a), the swelling strain is highly inhomogeneous within the circumference of the cladding. The difference between the maximal and minimal strain represents, in the non-coupled simulation, 40% of its average. As explained before, the temperature gradients are increased in the deformed geometry. Thus, in the coupled simulation, the difference between the maximal and minimal swelling strain within the cladding circumference is larger and represents a 50% of its average.

In Figure 6 b) and c), a qualitatively similar swelling distribution can be observed within the axial cladding slice in the coupled and in the non-coupled case. However, the coupling increases the swelling strain amplitude by 44%. This amplitude is higher than the one computed over a circumferential line (Figure 6 a) since the axial temperature gradients induce important axial swelling gradients too. It is worth noting that these axial gradients can only be correctly reproduced if the azimuthal gradients are considered, since the first are strongly “smoothed” out if the cladding temperature is considered homogeneous within its cross section.

Being able to correctly predict the swelling strain distribution is of particular importance, firstly, because it has been shown to produce excessive embrittlement of the cladding’s austenitic steel above approximately 2% [12]. Additionally, the swelling gradients give place to secondary stresses that, despite normally being relaxed by the irradiation creep [13], could also activate the damaging thermal creep.

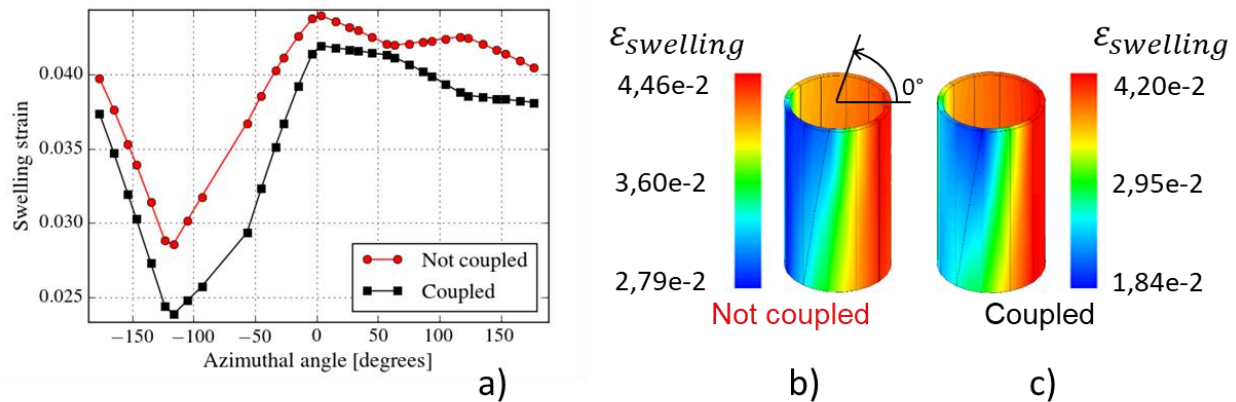


Figure 6: Swelling strain within the cladding circumference (a) and within a 1.5cm-long axial slice, with (c) and without coupling (b), at an axial position of 1.8 m.

CONCLUSIONS AND PERSPECTIVES

The irradiation of a 7-pin SFR fuel bundle was simulated with a novel coupled thermal-hydraulic/thermomechanical methodology. It has been shown that considering the coupling in the simulations leads, for a highly irradiated fuel bundle, to a significant reduction of the void swelling and the irradiation creep of the claddings, which are the main contributors to their diametral strain. These variables, averaged over the circumference of the cladding, were in very good agreement between a 3D and a beam-based representation of the fuel bundle, which encourages the use of the latter for larger bundle studies.

The computed strain reduction led to a decrease in the contact forces between pins, and thus to a significant reduction of the maximal equivalent stress. This is due to the delay of the 3rd phase of bundle mechanical interaction, which is not allowed during normal operation. Therefore, design margins could be increased by employing a coupled simulation approach.

Additionally, it was shown that considering the high temperature gradients computed with the detailed RANS approach leads to high swelling gradients, which are increased with the coupling. In particular, a coupled simulation led to a swelling strain amplitude over the circumference of the cladding

of about 50% of the average value at the same axial position, although this amplitude would be lower in a larger fuel bundle where the transition between the “cold” periphery and the “hot” centre is more progressive. This is relevant due to the swelling induced steel embrittlement and because of the secondary stresses associated to the swelling gradients. The authors are investigating this phenomenon with a more finely meshed 3D model required to this end.

In view of these results, the beam-based model was modified to allow considering the azimuthal temperature gradients, and the updated model will be available in the next version of DOMAJEUR2.

Additionally, a perspective of this work is to take advantage of the 3D model in a multiscale simulation approach, where it would be used to perform a detailed simulation of an area of interest identified by the beam-based model, which could also provide boundary conditions such as contact forces.

Finally, the high temperature and swelling gradients revealed by the use of the detailed RANS approach suggest that the methodology employed here could be used to determine more accurate material laws, which were established from experiences and simulations without taking these gradients or the coupling effects into account.

REFERENCES

- [1] K. Katsuyama, T. Nagamine, S. Matsumoto, and M. Ito, “Application of X-Ray Computer Tomography for Observing the Deflection and Displacement of Fuel Pins in an Assembly Irradiated in FBR,” *Journal of Nuclear Science and Technology*, vol. 40, no. 4, pp. 220–226, avril 2003.
- [2] F. Acosta, T. Cadiou, V. Blanc, and P. Rubiolo, “A new thermal-hydraulics thermomechanics coupling methodology for the modeling of the behavior of Sodium-cooled Fast Reactors fuel subassemblies under irradiation,” *Nuclear Engineering and Design*, acceptee 2019.
- [3] “STAR-CCM+ v12.02 Users Manual.” 2017.
- [4] T. Beck *et al.*, “Conceptual design of ASTRID fuel sub-assemblies,” *Nuclear Engineering and Design*, vol. 315, pp. 51–60, Apr. 2017.
- [5] T. Uwaba, M. Ito, and K. Maeda, “Diametral strain of fast reactor MOX fuel pins with austenitic stainless steel cladding irradiated to high burnup,” *Journal of Nuclear Materials*, vol. 416, no. 3, pp. 350–357, Sep. 2011.
- [6] *INTERNATIONAL ATOMIC ENERGY AGENCY, Structural Materials for Liquid Metal Cooled Fast Reactor Fuel Assemblies-Operational Behaviour, Nuclear Energy Series No. NF-T-4.3, IAEA, Vienna (2012).* .
- [7] M. Lainet, B. Michel, J.-C. Dumas, M. Pelletier, and I. Ramière, “GERMINAL, a fuel performance code of the PLEIADES platform to simulate the in-pile behaviour of mixed oxide fuel pins for sodium-cooled fast reactors,” *Journal of Nuclear Materials*, vol. 516, pp. 30–53, Apr. 2019.
- [7] T. Uwaba, M. Ito, S. Ukai, and M. Pelletier, “Development of a FBR Fuel Bundle-duct Interaction Analysis Code-BAMBOO,” *Journal of Nuclear Science and Technology*, vol. 42, no. 7, pp. 608–617, Jul. 2005.
- [9] A. Combescure, A. Hoffman, and P. Pasquet, “The CASTEM Finite Element System,” in *Finite Element Systems*, Berlin: Springer, 1982.
- [10] T. Uwaba, H. Ohshima, and M. Ito, “Analyses of deformation and thermal-hydraulics within a wire-wrapped fuel subassembly in a liquid metal fast reactor by the coupled code system,” *Nuclear Engineering and Design*, vol. 317, pp. 133–145, Jun. 2017.
- [11] T. Cadiou and F. Acosta, “The impact of the fuel pin bundle deformation on the thermal-hydraulics of ASTRID sub-assembly,” presented at the 12th International Topical Meeting on Nuclear Reactor Thermal-Hydraulics, Operation and Safety (NUTHOS-12), Qingdao, China, 2018.
- [12] F. Garner, “Irradiation Performance of Cladding and Structural Steels in Liquid Metal Reactors,” in *Materials Science and Technology*, American Cancer Society, 2006.
- [13] T. Uwaba and S. Ukai, “The secondary stress analyses in the fuel pin cladding due to the swelling gradient across the wall thickness,” *Journal of Nuclear Materials*, vol. 305, no. 1, pp. 21–28, Sep. 2002.